Journal of Nuclear Materials 437 (2013) 122–129

Contents lists available at SciVerse ScienceDirect

Journal of Nuclear Materials

journal homepage: www.elsevier.com/locate/jnucmat

The stability of alloying additions in Zirconium

S.C. Lumley [a,b], S.T. Murphy [a], P.A. Burr [a,c], R.W. Grimes [a], P.R. Chard-Tuckey [b], M.R. Wenman [a,*]

[a] Department of Materials, Imperial College, London, SW7 2AZ, UK
[b] Nuclear Department, Defence Academy, HMS Sultan, Gosport, Hampshire, PO12 3BY, UK
[c] Institute of Materials Engineering, Australian Nuclear Science and Technology Organisation, Menai, New South Wales 2234, Australia

ARTICLE INFO

Article history:
Received 2 November 2012
Accepted 26 January 2013
Available online 8 February 2013

ABSTRACT

The interactions of Cr, Fe, Nb, Ni, Sn, V and Y with Zr are simulated using density functional theory. Thermodynamic stabilities of various different Zr based intermetallic compounds, including multiple Laves phase structures and solutions of alloying additions in both α and β-Zr were investigated. The thermodynamic driving forces in this system can be correlated with trends in atomic radii and the relative electronegativities of the different species. Formation energies of Fe, Ni and Sn based intermetallic compounds were found to be negative, and the Zr_2Fe and Zr_2Ni intermetallics were metastable. Most elements displayed negative energies of solution in β-Zr but positive energies in the α-phase, with the exception of Sn (which was negative for both) and Y (which was positive for both). Solutions formed from intermetallics showed a similar trend.

1. Introduction

Zirconium is an element of crucial importance to the nuclear industry due to its use as a fuel cladding material in water cooled reactors. Its good corrosion resistance and low thermal neutron capture cross section make it the major component of a number of commercial alloys, including Zircaloy, Zirlo™ and M5™ [1]. A variety of different alloying elements are added to Zr in order to improve its resistance to creep, corrosion and its yield strength (see Table 1). In Zircaloy-4 Sn, Fe and Cr improve corrosion resistance, yield strength and creep resistance [3]. Older alloys, such as Zircaloy-2 also contain Ni, which was eventually removed because it increases the hydrogen pickup fraction [3]. Modern alloys such as Zirlo and M5 contain Nb, although this addition has been used in Russian and Canadian alloys for some time [1,2]. All the alloys mentioned here exhibit the low temperature, hexagonal-close-packed α-phase. β-phase Zr, with a body-centred-cubic structure is stable above 863 °C, although metastable β-phase Zr does exist below this temperature [4]. The β-phase, although not the primary component of in-reactor alloys, is still important as an intermediary phase during alloy processing.

In α-phase Zr the Sn forms a complete solid solution, whereas Fe, Cr and Ni exhibit more limited solubility (typically 50–170 ppm depending upon processing conditions [5,6]) and are found in addition-rich second phase precipitates (SPPs) [7]. These precipitates are typically between 100 nm and 1 μm in size, depending upon alloy composition and thermomechanical treatment [7]. Experimental evidence suggests that the majority of the Fe, Ni, and Cr resides in SPPs, with defined intermetallic compositions and structures. Nb also forms SPPs, however, these tend to be β-phase solid solution precipitates rather than intermetallic compounds with specific compositions. It has sometimes been reported that Fe will interact with Nb to form Zr–Nb–Fe precipitates [8]. The abundance, size and properties of all of these precipitates have a significant impact on alloy corrosion resistance, mechanical properties and the tendency of the alloy to absorb hydrogen [3,7–10].

Two primary structures of SPPs have been observed via microscopy; these are referred to as the Zr-rich and Laves phase precipitates (see Fig. 1). The Zr-rich phase contains primarily Ni and the Laves phases consists primarily of Cr, while both precipitates contain Fe [7]. Laves phase precipitates are part of a broad class of intermetallics, with three different structures, known as C14, C15 and C36 [11]. Precipitates containing only Fe and Zr, with no Cr, are also observed, though rarely [7,10]. Sn containing SPPs are occasionally observed, often associated with β-quenched samples, or as a result of irradiation [8]. SPPs have been noted to exist either in isolation, or in small clusters with Laves phase precipitates nucleating on existing Zr-rich precipitates [7]. Given the processing stages that a Zircaloy tube must go through, there are a number of potential points where SPPs can nucleate and grow. The first is when the Zircaloy is reheated (after casting from melt) to approximately 1050 °C and then quenched to manipulate the alloy texture. The second is during recrystallisation, which happens between a series of cold forming operations. A third and final possibility is during reactor operation, which may provide sufficiently high temperatures for precipitate growth, or may induce irradiation assisted precipitation [8].

* Corresponding author. Tel.: +44 (0)20 7594 6763; fax: +44 (0)20 7594 6729.
E-mail address: m.wenman@imperial.ac.uk (M.R. Wenman).

0022-3115/$ - see front matter © 2013 Elsevier B.V. All rights reserved.
http://dx.doi.org/10.1016/j.jnucmat.2013.01.335

Table 1
Commercial alloy compositions. The balance of composition is made up of Zr [1,37–39].

Alloy	wt%Sn	wt%Fe	wt%Cr	wt%Ni	wt%Nb	wt%V
Zircaloy 1	2.5	–	–	–	–	–
Zircaloy 2	1.5	0.15	0.1	0.05	–	–
Zircaloy 3	0.25	0.25	–	–	–	–
Zircaloy 4	1.2–1.7	0.18–0.24	0.07–0.13	70 ppm	–	–
Zirlo	0.7–1.5	0.07–0.14	0.03–0.14	0.03–0.14	0.5–2	–
M4	0.60	0.605	0.013	–	0.013	0.325
M5	30 ppm	237 ppm	32 ppm	–	≈1	–

It has also been reported that precipitates tend to shrink under neutron irradiation [8]. Different precipitates are known to shrink at different rates under different fluences and by different mechanisms. Ni rich precipitates show a tendency for Fe to leach out of the SPP until the whole precipitate dissolves into the bulk Zr [8]. Cr rich precipitates are known to amorphise, while both Fe and Cr diffuse out of the SPP [8]. Fe appears to diffuse faster than Cr, which leaves a Cr enriched zone around the SPP [9]. The phases that these different additions preferentially stabilise are an important component in the mechanisms of dissolution. This process is of particular interest, as the shrinkage of the precipitates is known to correlate with the rate of corrosion and oxide growth, which in turn is thought to correlate to hydrogen uptake [12].

In order to understand the formation and dissolution of precipitates, a grasp of the various thermodynamic driving forces at work is essential. A knowledge of the relative stabilities of the different phases may allow prediction of aspects of the life-cycle of these precipitates and by extension, the properties that they affect in the host alloy. In this study, the alloying elements Cr, Fe, Nb, Ni, Sn, V and Y are examined in Zr using Density Functional Theory (DFT) simulations. Atomistic scale techniques in general and DFT in specific, are usable over a large range of materials, and have demonstrated a degree of success when modelling alloys [13]. The thermodynamic driving forces for the formation of various intermetallic phases containing these elements are examined, as well as the solubilities of these elements and their intermetallic compounds in both α and β-Zr. This allows examination of the relative stabilities of various different phases in Zr alloys.

2. Methodology

All simulations were carried out using the CASTEP 5.5 simulation package [14]. CASTEP was selected on the basis that it relies on a plane wave pseudopotential description of electron basis sets. This description is ideal for modelling bulk crystals in situations where core electrons are relativity unaffected by the different bonding environments. It is important to select which electrons are modelled as non-interacting core electrons and which are modelled explicitly (valence electrons) by the DFT software. Here, the electrons considered as valence are:

- Cr – $3s^2 3p^6 4s^1 3d^5$.
- Fe – $4s^2 3d^6$.
- Nb – $4s^2 4p^6 5s^1 4d^4$.
- Ni – $4s^2 3d^8$.
- Sn – $5s^2 5p^2$.
- V – $3s^2 3p^6 4s^2 3d^3$.
- Y – $4s^2 4p^6 5s^2 4d^1$.
- Zr – $4s^2 4p^6 5s^2 4d^2$.

The pseudopotential scheme used is "on-the-fly" generation, in which an isolated all-electron calculation is carried out before the main calculation and used as a starting point to generate a pseudopotential. This was carried out for all pseudopotentials except Cr and V, as the default on-the-fly pseudopotentials for these elements required a much higher cut-off energy. Instead, standard ultrasoft pseudopotentials, as found in the CASTEP pseudopotential library, were used for Cr and V. All pseudopotentials (both on-the-fly and

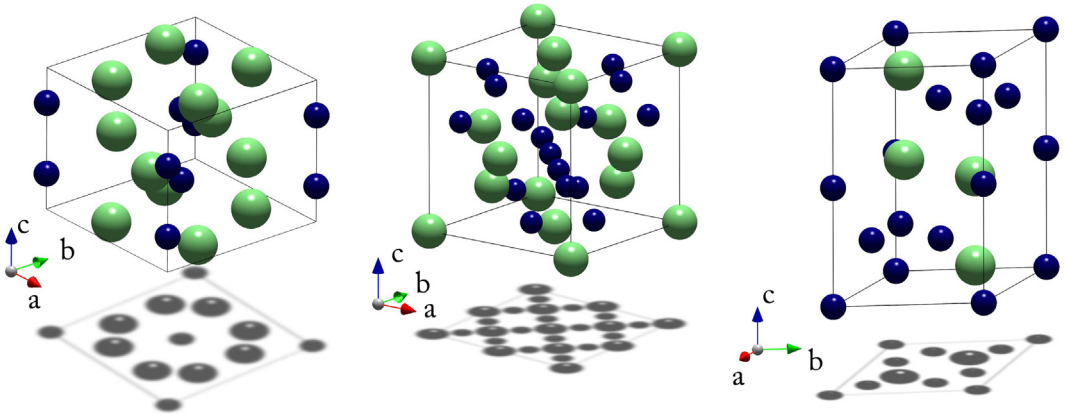

(a) The Zr-rich phase, with formula Zr_2M and structure archetype Al_2Cu.

(b) The cubic Laves phase (C-15), with formula ZrM_2 and structure archetype Cu_2Mg. This phase consists of a face-centred cubic lattice of Zr, with tetrahedral lattice sites alternately occupied with either another *Zr* atom or a sub-tetrahedron of M atoms.

(c) The hexagonal Laves phase (C-14), with formula ZrM_2 and structure archetype $MgZn_2$. The C-36 Laves phase is similar to the C-14 phase, except for being twice as long in the *c* axis, with the bottom half of the cell being a point reflection of the top half, through the centre of the cell.

Fig. 1. Crystal structures of the main precipitates found in Zr alloys. Zr is represented by the larger, light green spheres, and the alloying agent by the smaller, dark blue spheres. (For interpretation of the references to colour in this figure legend, the reader is referred to the web version of this article.)

Table 2
Lattice parameters of Zr phases and the various intermetallic phases studied in this work. Where available, literature values have been provided for comparison [48].

Species	Space group	Present work			Literature			Refs.
		a (nm)	*b* (nm)	*c* (nm)	*a* (nm)	*b* (nm)	*c* (nm)	
Pure αZr	$P6_3/mmc$	0.322	–	0.520	0.323	–	0.5145	[40]
Pure βZr	$Im\bar{3}m$	0.359	–	–	0.361	–	–	[35]
Pure ωZr	P6/mmm	0.506	–	0.312	0.503	–	0.311	[35]
C15 Laves $ZrCr_2$	$Fd\bar{3}m$	0.712	–	–	0.720	–	–	[41]
C14 Laves $ZrCr_2$	$P6_3/mmc$	0.505	–	0.814	0.511	–	0.831	[41]
Zr_2Cr (speculative)	I4mcm	0.657	–	0.537	–	–	–	–
Zr_3Fe	Cmcm	0.330	0.1086	0.885	0.332	0.1096	0.883	[42]
Zr_2Fe	I4mcm	0.625	–	0.563	0.638	–	0.559	[43]
C15 Laves $ZrFe_2$	$Fd\bar{3}m$	0.702	–	–	0.706	–	–	[44]
C14 Laves $ZrFe_2$	$P6_3/mmc$	0.498	–	0.811	–	–	–	–
Zr_2Ni	I4mcm	0.649	–	0.529	0.648	–	0.527	[43]
ZrNi	Cmcm	0.332	0.984	0.407	0.327	0.993	0.411	[45]
C15 Laves $ZrNi_2$	$Fd\bar{3}m$	0.696	–	–	0.692	–	–	[46]
C14 Laves $ZrNi_2$	$P6_3/mmc$	0.492	–	0.804	–	–	–	–
Zr_3Sn	$Pm\bar{3}n$	0.564	–	–	0.564	–	–	[47]
Zr_5Sn_3	$P6_3/mmc$	0.848	–	0.588	0.845	–	0.577	[32]
Zr_5Sn_4	$P6_3/mmc$	0.883	–	0.599	0.877	–	0.593	[32]
$ZrSn_2$	Fddd	0.570	0.965	1.00	0.564	0.957	0.993	[32]
Zr_2V (speculative)	I4mcm	0.746	–	0.568	–	–	–	–
C15 Laves ZrV_2	$Fd\bar{3}m$	0.738	–	–	0.692	–	–	[46]
C14 Laves ZrV_2	$P6_3/mmc$	0.523	–	0.847	–	–	–	–

library) are of the ultrasoft type [15], and so are compatible with each-other. Exchange–correlation was modelled using the Perdew, Burke and Ernzerhof formalisation of the Generalised Gradient Approximation [16].

A series of simulations were run to establish an appropriate basis set cut-off energy, and the density of sampling in the Brillouin zone. The results were converged to within two decimal places for a cut-off energy of 450 eV and a *k*-point spacing of 0.003 nm^{-1}. The *k*-points were arranged in a standard gamma centred Monkhorst–Pack grid [17]. In these simulations, and in all subsequent simulations, the energy of the electron wavefunctions was considered converged to a minimum value when the difference between successive iterations was below 10^{-6} eV/atom. Integration of the Brillouin zone was achieved using a cold smearing scheme (Methfessel–Paxton) [18], with a smearing parameter of 1 eV, in order to account for partial occupancies in the band structure. Simulations that varied this value by up to 0.9 eV found negligible difference in the final state of the system, so a higher value was chosen to speed convergence.

The simulations are static calculations, that is, they identify the minimum energy positions for atoms in a given structure and as such relate to zero temperature. When modelling cells, in order to find useful enthalpies and structural properties the starting structure was selected from literature values and the geometry of the system was allowed to relax, via a Broyden–Fletcher–Goldfarb–Shanno algorithm [19]. The positions of the ions, and the size and the shape of the cell boundaries are all allowed to relax. This is an appropriate scheme of relaxation, as the goal is to approximate a system with a limited concentration of alloying additions, after it has been allowed to reach equilibrium. The criteria for a successful iteration were selected as a balance between computational cost and numerical accuracy and are shown below:

- Energy derivative <0.001 eV.
- Force on ions <0.05 eV nm^{-1}.
- Displacement of ions derivative <0.001 nm.
- Total stress derivative <0.1 GPa.

When modelling defects, a $3 \times 3 \times 3$ supercell was used. In the case of α-phase Zr, this was created from the primitive hexagonal cell and in the case of β-phase Zr, the conventional unit cell. Both supercells contained 54 atoms. Although this choice introduces some anisotropy into the dimensions of the hexagonal system, it means that α and β-phase cells have an identical number of atoms, and hence identical alloying addition concentrations of 1.85 at.%. This concentration is useful, as the weight percent composition is appropriate to commercial alloys, particularly in the case of Sn, although it is still relevant with other alloying additions.

It is important to note that magnetic effects can have a substantial impact on overall lattice parameters and energies. Consequently care must be taken to ensure that the correct final magnetic state is converged upon. For all simulations carried out, this was achieved by setting the initial spin state of the system to the sum of individual formal spins of each of the present atoms and performing a spin polarised calculation. This produced reasonable magnetic configurations in most cases, with the exception of pure Cr. In order that the known magnetic state of Cr (antiferromagnetic) was achieved, it was necessary to specify the spin states of each atom individually, prior to convergence.

3. Results

3.1. Perfect crystals

It is important that the current calculations are able to reproduce experimental data concerning basic bulk properties, to provide confidence in simulated data for properties where there is little or no experimental data. Parameters calculated for the three polymorphs of Zr, are reported in Table 2, along with the relevant intermetallic phases. Most results are in excellent agreement with the available literature, especially those for Zr. These results also agree well with other relevant ab initio results [20,21].

Magnetic effects are again important, and in some cases, resulted in differences of over 1 eV per atom in formation energies, between the most favourable magnetic state, and a converged state when magnetic effects were not taken into account. As would be expected, Fe and Ni demonstrated strong ferro-magnetism, as well as all forms of Laves phase Fe intermetallics. Pure Cr, C14 and C36 Cr Laves phase intermetallic appear to be anti-ferromagnetic, while the C15 Laves phase and the Zr_2Cr intermetallics are weakly ferrimagnetic. The same is true of the Zr_2Fe precipitate, although it has been noted in other work that this phase has a somewhat

complicated magnetic structure [10]. Aside from this, all other simulation cells displayed no magnetic ordering.

3.2. Formation of intermetallics

The formation energies of different intermetallic phases provide a measure of their relative stability. Here, formation energies are defined as the enthalpy of forming a quantity of intermetallic compound from one unit of a composition weighted mixture of its constituent elements. Thus, the energy is given by:

$$E_{formation} = \frac{1}{x+y}E(\mathrm{Zr}_x\mathrm{M}_y) - \left(\frac{y}{x+y}E(\mathrm{M}) + \frac{x}{x+y}E(\mathrm{Zr})\right) \quad (1)$$

where $E(\mathrm{Zr}_x\mathrm{M}_y)$ is the energy of a cell simulating the intermetallic. The terms $E(\mathrm{M})$ and $E(\mathrm{Zr})$ represent the energies of a single atom from cells containing only the alloying agent and Zr respectively. In Fig. 2, the formation energies of various intermetallic phases are plotted against the composition of the intermetallic. It should be noted that the most stable intermetallic phase, or mixture of two intermetallic phases for any given composition, will occupy a point on a convex hull, drawn between the endpoints and lowest energy points of each series. If an intermetallic phase lies above this convex hull there will be a thermodynamic driving force for decomposition into a mixture of the two phases that bound the local segment of the convex hull. The ratio of these mixtures is determined by applying the lever rule. The convex hulls for Sn and Fe have been drawn on Fig. 2. Convex hulls have not been drawn for Cr and V due to the intermetallics displaying positive formation energies. The convex hull for Ni was not drawn as Ni forms a large number of different intermetallic phases in the Ni-rich portion of the Zr–Ni binary phase diagram, which were not modelled due to their irrelevance to Zr alloy compositions [22]. A convex hull for Ni intermetallics would not be reliable, without modelling these phases.

Fig. 2 shows that Fe, Ni and Sn based intermetallics all have negative enthalpies of formation, with the most favourable intermetallics being: C15 $ZrFe_2$, ZrNi, and Zr_5Sn_4. When Laves phase structures were modelled, Cr, Fe and Ni all favoured the C15 structure, followed by C36 and finally C14. For V based Laves phases, this order was reversed. Relative stabilities between C14 and C15 Laves phases are presented in Fig. 3. These were calculated by subtracting the formation energy (per formula unit) of the C14 variant from the C15 variant. A negative relative stability indicates a preference for the C15 structure, whereas a positive number indicates a preference for C14. These values are correlated with the metallic radius ratio between the two elements (R_{Zr}/R_M), and the valence electron concentration (VEC). The VEC is the modelled as the number of valence *s* and *d* electrons (as modelled in the pseudopotential) divided by the volume of a single formula unit of intermetallic. Previous studies of Laves phases have taken the VEC to be the number of *s* and *p* electrons per formula unit, however, this approximation does not accurately predict Laves phase stabilities for transition metal based Laves phases [11]. Instead, *s* and *d* electrons have been chosen, due to their importance in transition metal bonding, and a volume component has been added to account for the importance of electron density.

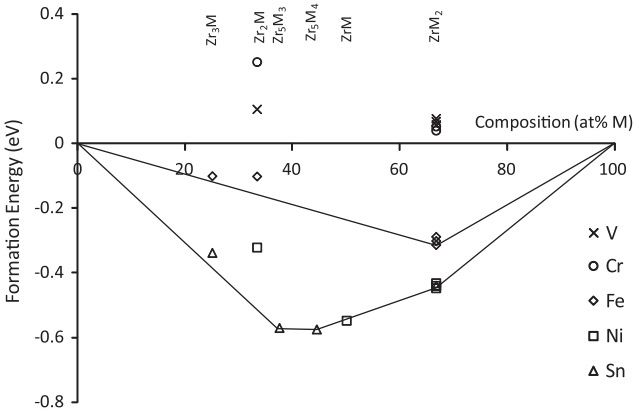

Fig. 2. Formation energy of different intermetallic phases, from their low temperature, single element phase constituents. Calculated using Eq. (1).

3.3. Solutions from single element phases

Solution energies of alloying elements in Zr are presented in Fig. 4. This energy indicates whether there is a thermodynamic driving force for either the element to segregate from Zr (positive values), or dissolve into the host matrix (negative values). For all elements, substitutional solution is examined, in which atoms of Zr are replaced by atoms of the alloying addition, with the Zr atoms forming new host lattice. For elements with a small metallic radii, that is Cr, V, Fe and Ni, interstitial solution was also considered, where the alloying additions occupy interstitial sites in the host matrix. Only the tetrahedral and octahedral interstitial sites are examined, as the other sites are too small to be viable; atoms placed at such sites will relax to tetrahedral or octahedral sites. Large atoms, such Nb, Sn and Y, were not considered for interstitial solution. The energy of solution for a substitutional site is given by the equation:

$$E_{solution} = \left(E(\alpha\mathrm{Zr}_{53}\mathrm{M}) + \frac{1}{54}E(\alpha\mathrm{Zr}_{54})\right) - \left(E(\alpha\mathrm{Zr}_{54}) + \frac{1}{x}E(\mathrm{M}_x)\right) \quad (2)$$

and the equation for interstitial solution is given by:

$$E_{solution} = E(\alpha\mathrm{Zr}_{54}\mathrm{M}_i) - \left(E(\alpha\mathrm{Zr}_{54}) + \frac{1}{x}E(\mathrm{M}_x)\right) \quad (3)$$

Solution calculations were carried out for α and β-phase Zr and compared (see Fig. 4). Most elements have a positive energy of solution in the α-phase and a negative energy of solution in the β-phase. Sn has a negative energy of solution in both the α-phase (-1.07 eV) and the β-phase (-1.54 eV). Conversely Y has a positive solution energy in both the α-phase (0.26 eV) and the β-phase (0.40 eV). Fe and Cr have lower solution energies in the α-phase when occupying an octahedral interstitial site, rather than a substitutional position (by 0.86 eV and 0.09 eV respectively). It should be noted that the solution energy of Ni on a tetrahedral site in the α-phase is not reported because it relaxed into the octahedral site. All the elements for which an interstitial site in the β-phase was investigated exhibit a preference for interstitial solution. The energy of substitution for V in the β-phase, -0.02 eV, is so small it is not readily apparent in Fig. 4.

The volume associated with each defect was also calculated and is presented in Fig. 5. The self interstitial volumes for Zr are also shown. Defect volumes are simply the difference in volume between a defective cell and a Zr supercell. As such, they correspond to volumes per atom but at a specific defect concentration of 1.85 at.% (as do the solution energies). These values are plotted against the metallic radii of the different elements. The metallic radius for each element was calculated from its single element phase, as simulated in this study (assuming a simple contacting sphere model). As this investigation involves two different phases of Zr, the appropriate metallic radius for each phase is different, and has been plotted as such. Linear regression trend lines are displayed in Fig. 5 for all defect types. These display a positive linear relationship. The trend lines for substitutional defects in the α and β-phase cross the *x* axis at 0.159 nm and 0.155 nm, which are

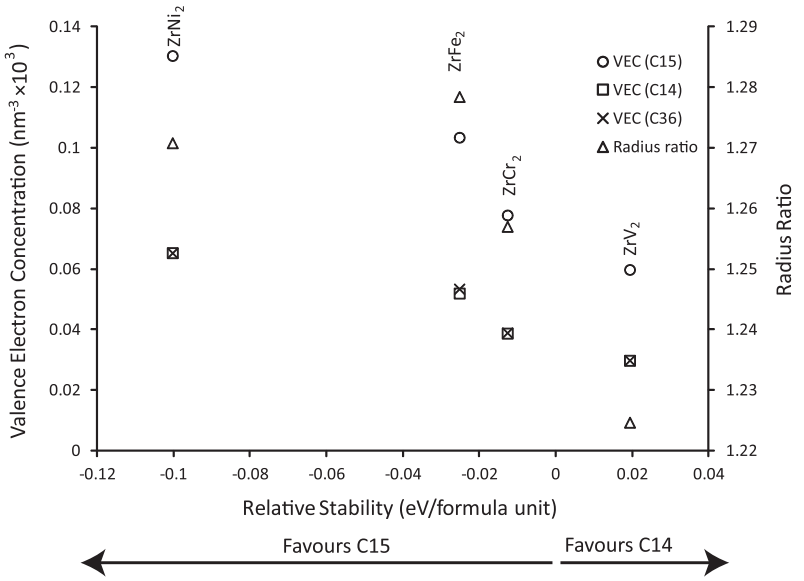

Fig. 3. Relative stabilities of two different ZrM_2 Laves phases, plotted against values representing the geometric (radius ratio, R_{Zr}/R_M) and electronic (valence electron concentration) components of Laves phases stability. Radius ratio is plotted on the secondary axis, while VEC is plotted on the primary. The VEC for the C36 Laves phase is almost identical to that of the C14.

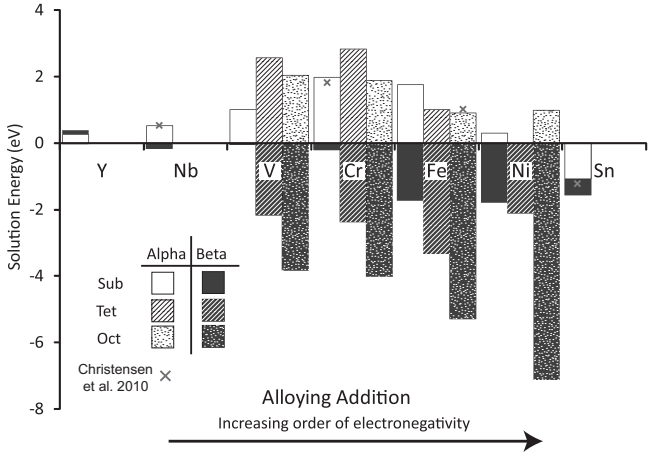

Fig. 4. Solution energies of different single phase elements, on different sites in α and β-Zr, as calculated by Eqs. (2) and (3). Values calculated by Christensen et al. can be found in [31]. Elements are arranged in increasing order of electronegativity, although the horizontal axis is not scaled. The electro-negativity of Zr sits between Y and Nb [29].

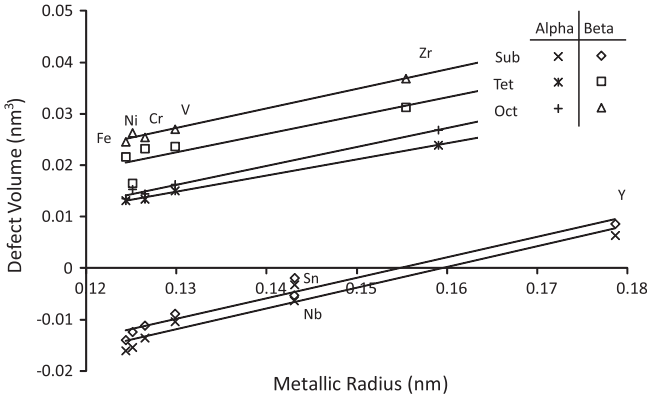

Fig. 5. Defect volumes of the different elements in various different sites of α and β-phase Zr. Metallic radii were calculated from the relaxed, single phase element.

respectively the calculated metallic radii for α and β-phase Zr. All interstitial defects show much greater defect volumes than in substitutional alloys. The elements Sn and Nb have similar metallic radii, hence they are difficult to distinguish in Fig. 5 (the results for Sn lie above those for Nb).

3.4. Solutions from intermetallics

When considering a real alloy system, it is important to appreciate that it may not be a single element phase that is dissolving into the host matrix. As discussed above, most of the elements investigated here form intermetallic phases, consequently the reaction of interest is not necessarily between a pure species and a solution but between an intermetallic phase and a solution. The solution energy of a general intermetallic phase onto a substitutional site in the host lattice is given by:

$$E_{solution} = \left(E(\alpha Zr_{53}M) + \left(\frac{y}{x}+1\right)E(\alpha Zr)\right) - \left(E(\alpha Zr_{54}) + \frac{1}{x}E(M_xZr_y)\right) \quad (4)$$

or if the solution is interstitial:

$$E_{solution} = \left(E(\alpha Zr_{54}M_i) + \frac{y}{x}E(\alpha Zr)\right) - \left(E(\alpha Zr_{54}) + \frac{1}{x}E(M_xZr_y)\right) \quad (5)$$

The solution energies of Cr, Fe, Ni, Sn and V dissolved from their intermetallic phases are presented in Fig. 6. The solution energy of the most favourable site in each phase is used, as determined from Fig. 4. The trends in Figs. 4 and 6 are similar; that is, elements displaying a positive solution energy from a single element phase into α-Zr, will display a positive intermetallic solution energy. The same follows for β-phase Zr. Sn has a comparatively low solution energy in the α-phase and a comparatively high energy in β-phase; it is the only element where an intermetallic possesses a negative solution energy in α-phase Zr.

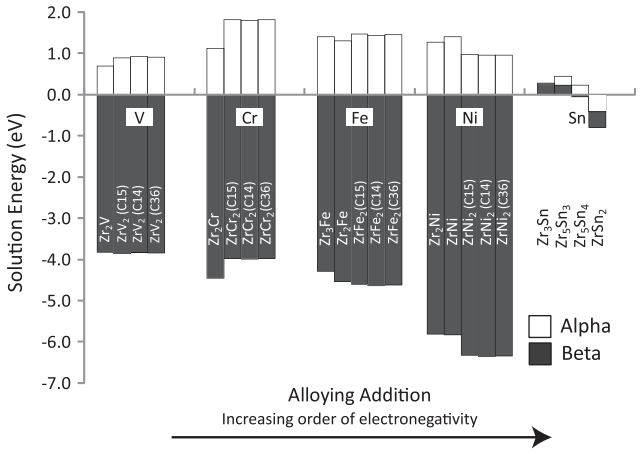

Fig. 6. Solution energies of different intermetallics in Zr, as calculated by Eqs. (4) and (5). The site chosen for solution was based upon the most favourable site, as shown in Fig. 4.

4. Discussion

4.1. Intermetallic formation

Fig. 2 indicates that the general order of increasingly negative intermetallic formation energy (excluding Zr_2Cr and Zr_2V for reasons discussed below) is V, Cr, Ni, Fe, and finally, Sn. With the exception of Fe and Ni, this is consistent with the Hume-Rothery rules, that is, the greater the difference between the two elements' electronegativities, metallic radii, or native crystal structures, the greater the likelyhood of intermetallic compound formation rather than a solid solution [23]. The positions of Fe and Ni in this order are reversed, possibly because they have very similar electronegativities (and metallic radii), suggesting that another factor is contributing. In fact, single phase Fe, Ni and some of their associated intermetallics display distinct magnetic structures. Magnetism will stabilise some phases over others, and magnetic effects are not referred to in the Hume-Rothery rules. Other than Fe and Ni, the greater the difference in electronegativity between an alloying addition and Zr, the more stable the intermetallic.

In this study, two speculative intermetallics have also been investigated; Zr_2Cr and Zr_2V. Although Cr and V form ZrM_2 Laves phases, they are not known to form Zr_2M Zr-rich precipitates, despite the fact that this structure is commonly formed with Fe and Ni. The formation energies for Zr_2Cr and Zr_2V were found to be substantially positive (0.75 eV and 0.31 eV respectively) suggesting that they are not stable and the absence of these structures in existing phase diagrams and commercial alloys is due to thermodynamic instability, rather than poor kinetics during formation.

It can be seen in Fig. 2 that the Cr and V based Laves phase intermetallics have slightly positive energies of formation. This would suggest that these phases are not stable, however, it does not necessarily rule out their formation. The binary phase diagrams of Cr and V with Zr show that the Laves phase is particularly non-stoichiometric [24,25]. As a result, the system configurational entropy will increase considerably, when moving from two pure substances, to a single non-stoichiometric intermetallic phase; such an increase in entropy could be sufficient to drive the reaction. This is particularly important when considering the actual SPPs, as a $Zr(Fe,Cr)_2$ intermetallic is observed. It is possible that the more stable Fe based Laves phase stabilises its Cr counterpart to some degree.

The Zr_2Fe phase, does not lie on the Zr–Fe convex hull. Consequently this phase is metastable and would decay into a mixture of Zr_3Fe and $ZrFe_2$ under equilibrium conditions. A similar finding has been reported previously and typically, the Zr_3Fe phase is only observed in Fe rich alloys [10]. The Zr_2Fe phase is readily observed as a component of $Zr_2(Fe,Ni)$ precipitates, in alloys containing Ni. Thus, two mechanisms are suggested that may play a role in its stabilisation. First, that the phase cannot decompose due to kinetics. This is reasonable as the alloy is quench cooled. Second, the corresponding Ni based intermetallic has a lower enthalpy of formation and may assist in stabilising the Zr_2Fe phase. If Ni stabilises the Zr_2Fe phase, (or even vice versa), we would expect bringing the two intermetallics together to have a significant enthalpy of mixing, in order to offset their individual metastabilities. This mechanism is consistent with experimental results published by Barbaris et al. [10], who observed that Zr_2Fe is significantly more common in alloys containing Ni. Further work on mixed intermetallic phases may allow development of these ideas. The formation of one intermetallic in preference of another has significant impacts in terms of hydride resistance, as the $Zr_2(Fe,Ni)$ phase has been noted to provide preferential solution sites for hydrogen [30].

The formation of a Laves phase and the preferential stability of a particular Laves phase have two main predictive aspects. The first is a geometric component relating to the difference in size between the two atoms, while the second is an electronic component, relating to the concentration of valence electrons, the VEC as discussed earlier [26]. With regard to the geometric component, Laves phases tend to be more stable as the radius ratio between the two elements approaches 1.225 [27]. In Fig. 3, the Laves forming additions have ratios between 1.21 and 1.29. V is the only element which preferentially forms a C14 structure, and this element has a ratio below the ideal value. With regard to the electronic component, Fig. 3 shows that as the VEC decreases, there is a tendency for C14 structures to be favoured over C15. The implication is, that for this system C14 is more suitable for large and electrically diffuse alloying additions. However, the relative stabilities of different Laves phases are notoriously difficult to predict from first principles [11], consequently, the previous statement is probably not a rule that can be reliably applied outside this system.

4.2. Solution energies

4.2.1. Solutions from single elements

In the α-phase, Cr and Fe prefer to occupy interstitial sites, while all other atoms occupy substitutional sites. This is not surprising as Cr and Fe are the smallest atoms considered. The octahedral interstitial site is predicted to be the most favoured, most likely because it is the largest site by volume in which to insert an atom. In a simple contacting-spheres model, the tetrahedral and octahedral sites in α-phase Zr have radii of 0.035 nm and 0.065 nm respectively [28]. The metallic radii of Cr and Fe are 0.125 nm and 0.124 nm [29], however as both are slightly more electronegative than Zr (respectively, 1.66 and 1.83 Pauling units, compared to 1.33 of Zr), these additions will be "larger" still, due to having gained electrons at the expense of Zr. Therefore, Cr and Fe atoms can only fit into the interstitial sites with a significant volume change of the cell, as shown in Fig. 5. This volume change is an important consideration with regards to the solution energy, as demonstrated in a comparison of the values determined during this study, and the values given by Christensen et al. [31]. Unlike the present study, Christensen et al. did not allow the boundaries of the periodic cells to relax, constraining the cell volume and aspect ratio. As a result, the present study finds a lower solution energy for Fe in α-phase Zr, as well as finding that Cr, prefers an interstitial, over a substitutional site. As this investigation centres on the impact of a given concentration of an alloying addition in a Zr lattice, it is necessary to allow the lattice to accommodate the strain caused by the defect.

In the β-phase, all the elements for which interstitial sites were considered showed preference for an interstitial site over a

substitutional site. Unlike HCP, the BCC structure is not close packed and therefore its interstitial sites are larger. To compare, the octahedral site in α-Zr is 0.130 nm across, while in β-Zr it is 0.193 nm across in the *ab* plane, though only 0.048 nm along the *c*-axis. This is because the four atoms in the *ab* plane are in [1 1 0] directions whereas the two in the *c*-axis are in [0 0 1] directions. During relaxation, these two atoms are pushed out along [0 0 1] directions, while the cell experiences a slight contraction in the other two directions. Overall, this is responsible for the large defect volumes shown in Fig. 5.

Except for Sn, all elements exhibit positive solution energies in α-phase Zr, in-keeping with observations that these elements do not remain in solid solution under equilibrium conditions [10]. Sn is the only element that exhibits a negative solution energy and the only element in this study that forms an α-phase Zr solid solution. Sn is known to stabilise α-Zr, and this effect can be seen clearly on the Zr–Sn binary phase diagram [32], as the phase boundary between the α and β-phase Zr increases in temperature as Sn content is increased. A similar observation can be made with Nb. The Zr–Nb binary phase diagram shows that Nb exhibits complete solid solubility in the β-phase and little solubility in the α-phase [33] (although metastable solubility under irradiation has been reported [34]). The results here show a positive solution energy in the α-phase, but a negative energy in the β-phase. The Nb case is particularly clear, because Nb does not form intermetallic compounds with Zr in a binary system, hence intermetallic reactions do not need to be considered when examining solubility.

As in the case of formation energies, the difference in electronegativity between Zr and a given alloying addition gives rise to a correlation in how stable the alloying addition is in solution. In Fig. 4 for the β-phase, the trend is that a greater difference in electronegativity results in a greater energy of solution, with the exception of Sn. As the only non-transition metal in the selection of elements here, the difference in behaviour can be ascribed to the different bonding character.

Some correlations with behaviour under irradiation can also be noted. It has been observed that Fe–Cr SPPs tend to dissolve more quickly than Fe–Ni SPPs, and in the latter case, the Fe leaches out of the SPP before the Ni [12]. With Fe and Cr both occupying interstitial sites, there are more readily accessible sites for them to occupy in the Zr matrix, thus Fe and Cr can dissolve into Zr faster than an addition that requires a substitutional site to become available, such as Ni. Nevertheless, Cr dissolves slower then Fe [9]. As Fe has a lower solution energy in the α-phase than Cr (by 0.98 eV), there is a greater driving force for Fe to dissolve. It may be that Fe atoms, given their large defect volume, block adjacent sites from being occupied by other interstitial solutes due to the associated lattice strain field, thus slowing the solution of Cr. It is also notable that the tetrahedral and octahedral sites for Fe are very similar in energy, whereas those for Cr are not. If the lowest energy diffusion pathway involves both sites, this may be consistent with a lower migration activation energy for Fe than Cr, although it would be necessary to calculate the actual migration barrier energy before a definitive statement can be made.

With regards to the defect volumes shown in Fig. 5, atoms with a greater difference in size, with respect to Zr, distort the lattice more when substituted into a Zr lattice. The relationship between metallic radius and defect volume is linear, with each defect site showing near parallel trends. The α-phase Zr defect volumes are always lower than the corresponding β-phase values. The α-phase is a stiffer structure, with higher elastic constants, so it is reasonable to expect the α-phase to resist volume change more than the β-phase [35]. As would be expected, the metallic radius predicted when the defect volume equals zero is the same as the metallic radius of Zr in the host lattice. That most elements show good agreement with the linear relationships is consistent with geometrical factors being dominant in determining lattice strain in this system due to single alloying additions.

Fig. 5 shows that Sn lies slightly above the trend lines in α and β-phase Zr. This is an indication that bonding effects, or electron transfer is making the Sn atom appear "bigger" than would otherwise be expected. This could be due to the fact that Sn is the element in this study with the greatest electronegativity difference with respect to Zr. Fig. 5 also indicates that Ni has an unusually low defect volume when it occupies a tetrahedral site in β-Zr, which coincides with a comparatively high solution energy for Ni on this site. It is not clear why Ni exhibits this behaviour specifically on the tetrahedral site, however, as this is not the most favourable site (by a significant margin), it will not have any impact on conclusions drawn.

4.2.2. Intermetallic solutions

Fig. 6 indicates that most intermetallic phases have positive solution energies in α-Zr. Conversely, the extremely negative solution energies in β-Zr, suggest that these intermetallics would not coexist with the β-phase at the concentrations examined here, instead favouring solution. The implication of this is that the formation of SPPs will be critically dependent on details of the $\beta \rightarrow \alpha$ phase change during processing, as is well known.

Sn intermetallics demonstrate much lower solution energies into α-Zr than those of other alloying additions, ranging from 0.45 eV (favouring intermetallic formation) to −0.41 eV (favouring solid solution). Thus, even when the enthalpy for intermetallic formation is favourable, it is small. Therefore, at temperatures where the material is processed (and used) configurational entropy will likely drive solid solution formation. However, under substantial irradiation, some Sn based precipitates have been reported [8,36]. If sufficient Sn could diffuse together, (via radiation assisted migration) then this study is consistent with these precipitates being stable at lower temperatures.

5. Conclusions

The simulations support the following conclusions:

- Overall, much of the behaviour of this system can be understood in terms of simple trends in energy and defect volume as a function of the electronegativities, metallic radii or valence electron concentrations of the alloying elements.
- Formation energies for intermetallic phases show that some compounds are stable, while others are metastable. In particular, Zr_2Fe and Zr_2Ni are metastable, although Zr_2Ni has a more negative formation energy. It may be that the presence of the Zr_2Fe phase in Zr alloys is a result of kinetics rather than thermodynamics. It is also likely that the corresponding Ni and Fe phases stabilise each other to some degree.
- Speculative Zr_2Cr and Zr_2V intermetallics have substantially positive formation energies, implying they are not stable.
- There is an energetic preference for Cr and Fe to reside on interstitial sites, rather than substitutional sites. With all additions, an interstitial alloy produces a significant, anisotropic lattice strain.
- Defect volumes for the different elements correlate well with metallic radii, with some anomalies regarding Sn (which has a larger volume than expected) and Ni (which shows a smaller volume than expected when on the less stable tetrahedral interstitial site).
- Most alloying additions show limited solubility (from their single phase metals) in α-Zr, but much greater solubility in β-Zr. The same is true for solutions from corresponding Zr intermetallics.

- Sn shows solubility in both α and β-Zr. However, most Sn intermetallics, show only a marginally positive solution energy, meaning they are likely to be soluble at elevated temperatures.
- Y, which does not form a stable intermetallic with Zr and has little equilibrium solubility in both α and β-Zr.
- Nb does not form a stable intermetallic and has little equilibrium solubility in α-Zr. However, unlike Y, Nb is soluble in β-Zr.

In general, these conclusions are in agreement with experimental observations where available. However, many of the specific energies or defect volumes have not been previously established, or have been arrived at by disparate methods so as to hinder comparison. While these numbers provide a useful body of data, much remains to be done, especially since kinetic effects are important, as are the interplays between multiple alloying additions.

Acknowledgements

The Imperial College High Performance Computing centre is acknowledged for providing assistance and computational resources. S.C. Lumley thanks the Ministry of Defence for providing funding. M.R. Wenman acknowledges a research fellowship from EDF Energy.

References

[1] K. Lingamurty, I. Charit, Prog. Nucl. Energy 48 (4) (2006) 325–359.
[2] B.A. Cheadle, The development of Zr 2.5Nb pressure tubes for CANDU reactors, in: 16th International Symposium on Zirconium in the Nuclear Industry, 2010, pp. 67–87.
[3] G.P. Sabol, ZIRLO™ – An alloy development success, in: 14th International Symposium on Zirconium in the Nuclear Industry, 2005, pp. 3–24.
[4] J.P. Abriata, J.C. Bolcich, Bull. Alloy Phase Diagrams 3 (1) (1982) 28.
[5] C. Li, J. Nucl. Mater. 304 (2–3) (2002) 134–138.
[6] H. Zou, G.M. Hood, J.A. Roy, R.H. Packwood, V. Weatherall, J. Nucl. Mater. 208 (1994) 159–165.
[7] P. Chemelle, D.B. Knorr, J.B. Van-Der-Sande, R.M. Pelloux, J. Nucl. Mater. 113 (1983) 58–64.
[8] M. Griffiths, R. Gilbert, G.J.C. Carpenter, J. Nucl. Mater. 150 (1) (1987) 53–66.
[9] R. Adamson, Recovery of Irradiation Damage by Post-Irradiation Thermal Annealing Relevance to Hydrogen Solubility and Dry Storage Issues, Tech. Rep. 3, Electric Power Research Institute (US), Palo Alto, California, 2006.
[10] P. Barbaris, N. Dupin, C. Lemaigan, A. Pasturel, M.J. Grange, Thermodynamics and kinetics of Zr–Cr–Fe–Ni alloys, in: 14th International Symposium on Zirconium in the Nuclear Industry, 2005, pp. 129.
[11] F. Stein, M. Palm, G. Sauthoff, Intermetallics 12 (7–9) (2004) 713–720.
[12] S. Valizadeh, R.J. Comstock, M. DahlBack, G. Zhou, J. Wright, L. Hallstadius, J. Romero, Effects of secondary phase particle dissolution on the in-reactor performance of BWR cladding, in: 16th International Symposium on Zirconium in the Nuclear Industry, 2010.
[13] J. Hafner, Acta Mater. 48 (1) (2000) 71–92.
[14] S.J. Clark, M.D. Segall, C.J. Pickard, P.J. Hasnip, M.J. Probert, K. Refson, M.C. Payne, Z. Kristallogr. (220) (2005) 567–570.
[15] D. Vanderbilt, Phys. Rev. B 41 (11) (1990) 7892–7895.
[16] J.P. Perdew, K. Burke, M. Ernzerhof, Phys. Rev. Lett. 77 (18) (1996) 3865–3868.
[17] H. Monkhorst, J. Pack, Phys. Rev. B 13 (12) (1976) 5188–5192.
[18] M. Methfessel, A. Paxton, Phys. Rev. B 40 (6) (1989) 3616–3621.
[19] B.G. Pfrommer, M. Cote, G.S. Louie, M.L. Cohen, J. Comput. Phys. (131) (1997) 133–140.
[20] C. Domain, R. Besson, A. Legris, Acta Mater. 50 (13) (2002) 3513–3526.
[21] Y. Udagawa, M. Yamaguchi, H. Abe, N. Sekimura, T. Fuketa, Acta Mater. 58 (11) (2010).
[22] H. Okamoto, J. Phase Equilib. Diffus. 28 (4) (2007) 409.
[23] W. Hume-Rothery, B.R. Coles, Atomic Theory for Students of Metallurgy, fifth ed., The Institute of Metals, (1969).
[24] H. Okamoto, J. Phase Equilib. Diffus. 14 (6) (1993) 768.
[25] H. Okamoto, J. Phase Equilib. Diffus. 27 (5) (2006) 543–544.
[26] R. Ferro, A. Saccone, Intermetallic Chemistry, first ed., Pergamon-Elsevier Science Ltd., 2008.
[27] P. Villars, L. Calvert, Pearson's Handbook of Crystallographic Data for Intermetallic Phases, American Society of Metals, 1985.
[28] C. Hammond, Introduction to Crystallography, Oxford University Press, 1992.
[29] CRC, Handbook of Chemistry and Physics, 80th ed., CRC Press LLC, 1999.
[30] P.A. Burr, S.T. Murphy, S.C. Lumley, M.R. Wenman, R.W. Grimes, Hydrogen accommodation in Zr second phase particles. Implications for H pick-up and hydriding of Zircaloy-2 and -4. Corros. Sci., in press, doi: 10.1016/j.corsci.2012.11.036.
[31] M. Christensen, T.M. Angeliu, J.D. Ballard, J. Vollmer, R. Najafabadi, E. Wimmer, J. Nucl. Mater. 404 (2) (2010) 121–127.
[32] R. Jerlerudperez, C. Toffolonmasclet, J. Joubert, B. Sundman, Calphad 32 (3) (2008) 593–601.
[33] H. Okamoto, J. Phase Equilib. Diffus. 13 (5) (1992) 577.
[34] M. Griffiths, H. Muellejans, Micron 26 (6) (1995) 555.
[35] S. Banerjee, P. Mukhopadhyay, Phase Transformations: Examples from Titanium and Zirconium Alloys, Elsevier, 2007.
[36] T.Y. Yang, G.P. Yu, L.J. Chen, J. Nucl. Mater. 150 (1987) 67–77.
[37] R.L. Schulte, E.A. Kamykowski, J. Radioanal. Chem. 43 (1) (1978) 233–242.
[38] M. Ahmad, J.I. Akhter, M.A. Shaikh, M. Iqbal, W. Ahmad, J. Mater. Eng. Perform. 12 (April) (2003) 179–182.
[39] S. Doriot, D. Gilbon, J. Bechade, M. Mathon, L. Legras, J. Mardon, Microstructural stability of M5™Alloy irradiated up to high neutron fluences, in: 14th International Symposium on Zirconium in the Nuclear Industry, 2004, pp. 175–201.
[40] J. Goldak, L.T. Lloyd, C.S. Barrett, Phys. Rev. 144 (2) (1966) 480–484.
[41] J.L. Soubeyroux, M. Bououdina, D. Fruchart, L. Pontonnier, J. Alloys Compd. 219 (1995) 48–54.
[42] P. Matkovic, T. Matkovic, I. Vickovic, Metalurgija 29 (1) (1990) 3.
[43] E.E. Havinga, H. Damsma, P. Hokkeling, J. Less Common Met. 27 (2) (1972) 169–186.
[44] P. Warrentt, J.B. Forsythl, G.J. Mcintyre, N. Bernhoeftt, J. Phys.: Condens. Matter 4 (26) (1992) 5795.
[45] M. Bououdina, B. Lambert-Andron, B. Ouladdiaf, S. Pairis, D. Fruchart, J. Alloys Compd. 356–357 (2003) 54–58.
[46] J.M. Oliveira, D.C. Brochado, I.R. Harris, J. Mater. Sci. 18 (12) (1983) 3649–3660.
[47] V. Baykov, R. Perez, P. Korzhavyi, B. Sundman, B. Johansson, Scripta Mater. 55 (5) (2006) 485–488.
[48] D.A. Fletcher, R.F. McMeeking, D. Parkin, The United Kingdom Chemical Database Service, J. Chem. Inf. Comput. Sci. 36 (1996) 746–749.